Absorption of Pulsed Terahertz and Optical Radiation in Earthworm Tissue and Its Heating Effect

Mahmoud H. Abufadda[1,2] · **Nelson M. Mbithi**[1,3] · **Gyula Polónyi**[3,4] ·
Priyo S. Nugraha[3,4] · **Andrea Buzády**[1] · **János Hebling**[1,3,4] · **László Molnár**[2] ·
József A. Fülöp[1,3,5]

Abstract

The transmission of THz, near-infrared (1030 nm), and green (515 nm) pulses through *Eisenia andrei* body wall is studied, which consists of epithelial layer and circular and longitudinal muscles. Samples with the full-body cross-section were also investigated. The transmitted power for the green pulses followed the Beer-Lambert law of exponential attenuation for all thicknesses and tissue structures. Different body wall and body center absorption coefficients were found in case of infrared pulses. In the THz range, the body wall absorption coefficient steadily increases from about 80 cm^{-1} at 0.2 THz to about 273 cm^{-1} at 2.5 THz. Numerical estimation indicates that THz pulses of 5-μJ energy and 1-kHz repetition rate (5-mW average power) cause only a small temperature increase of about 0.4 K, suggesting that heating has minor contribution to biological effectiveness.

1 Introduction

Electromagnetic waves influence the activity of distinct cells and tissues of various species suggesting that probably all life forms respond to light [1]. Because of the possible biomedical applications, the photobiomodulation effect of certain

✉ József A. Fülöp
  fulop@fizika.ttk.pte.hu

1 Institute of Physics, University of Pécs, Pécs 7624, Hungary

2 Institute of Biology, University of Pécs, Pécs 7624, Hungary

3 Szentágothai Research Centre, University of Pécs, Pécs 7624, Hungary

4 MTA-PTE High-Field Terahertz Research Group, Pécs 7624, Hungary

5 ELI-ALPS, ELI-HU Nonprofit Ltd., Szeged 6728, Hungary

electromagnetic waves, e.g., laser light (for review, see Ref. [2]) or terahertz (for review, see Ref. [3]) is intensively investigated in in vitro and in vivo experimental models. Biological effects of terahertz (THz) radiation have been extensively studied at various levels, from molecules [4, 5] to the organism [6]. Due to the complexity of biological materials, in many cases, it has been difficult or impossible to draw more general conclusions which go beyond the scope of a specific type of samples. For more complex samples, such as tissues, this is even more so.

With the increasingly widespread use of intense pulsed THz sources, the systematic study of their biological effects became more important and timely. Still, widely recognized, precise irradiation standards according to biological effectiveness are not yet available. To set up such standards can be very challenging as THz pulses can interact with biological materials in many different ways [7, 8].

One of the simplest ways of characterizing the interaction of THz radiation with biological tissues is to measure the dissipation of power by propagation through the sample. This can deliver very useful information, for example, on heating and other biological effects. Information about the (frequency-dependent) optical properties of tissue in the THz range, obtained, for example, by time-domain THz spectroscopy, is highly relevant for biomedical applications [9]. In case of human tissue, medical and related applications include in vivo clinical imaging, e.g., for burns and skin cancer identification, optimization of acquisition or irradiation protocols, and supplying data to reveal the interaction mechanisms. Skin, adipose tissue, striated muscle, vein, nerve, and blood were measured by THz spectroscopy [10]. The penetration depth of visible (laser) light into human skin tissue strongly depends on wavelength and skin pigmentation [11]. Similar finding was reported from the measurement of the optical properties of in vitro–pigmented human skin tissue models [12]. The degree of cell differentiation and type of donor (Asian, Black, and Caucasian) both contribute to the measured THz optical properties.

Recently, new experimental organisms, earthworm species, have been introduced to investigate wound healing [13, 14] and segment regeneration [6]. In our previous study, a very pronounced effect of illumination of earthworms by THz pulses was found on the regeneration of ablated tail segments in *Eisenia andrei* earthworms [6]. Namely, illumination by THz pulses resulted in a significant acceleration of the regeneration process. In contrast, illumination by green or near-infrared pulses did not result in such effect. In order to help to clarify the reason for this, it is necessary to determine the intensity of the different radiations at different depths of the animals, where different tissues are located. Based on the result of transmission measurements, it is possible to calculate the radiation intensity at different depths within the earthworm.

In this study, the transmission of THz pulses through earthworm tissues is studied. Body wall samples were taken from *Eisenia andrei* earthworms of different sizes, consisting of epithelial layer and circular and longitudinal muscles. Also samples of larger thickness, containing the complete cross-section of the animal, were investigated for comparison. The power transmission results for THz pulses are compared to those for near-infrared (1030 nm) and green (515 nm) pulses. The measured THz transmission data are used to estimate the temperature increase caused by intense THz pulse irradiation assuming parameters similar to those applied in our previous

study [6]. The knowledge of the heating effect can be relevant for the estimation of its biological effectiveness. In context of our previous study [6], the goal of this work is to rule out heating as the reason of the observed dramatic biological effect.

2 Materials and Methods

2.1 Optical and THz Transmission Measurements

The experimental setup is shown in Fig. 1. Three different sample positions allowed to switch quickly between the three types of irradiation pulses. The infrared (IR) laser pulses of 1030-nm central wavelength, 180-fs pulse duration, up to 1-mJ pulse energy, and controlled intensity were delivered to position IR (Fig. 1) by an Yb:KGW regenerative amplifier operating at 1-kHz repetition rate. Before the sample, an iris diaphragm reduced the beam size to about 2 mm, a diameter smaller than the sample size. Green laser pulses of 515-nm wavelength were produced by phase-matched second-harmonic generation of the infrared laser pulses in a BBO crystal. Reflection on a dichroic mirror was used to separate the green light from the infrared fundamental and to direct it to position G (Fig. 1) through another 2-mm iris aperture. The infrared and green laser powers, transmitted through the sample and the sample holder glass plate, were measured by a laser power meter (Gentec, model XLP12-3S-H2-D0). To obtain transmission values, reference measurements with the sample holder plate were carried out.

THz transmission measurements were carried out in a commercial time-domain THz spectrometer (TDTS) of model Tera K8 manufactured by Menlo Systems. Nearly-single-cycle THz pulses were generated in the TDTS with a biased photoconductive antenna illuminated by femtosecond laser pulses. The TDTS configuration was similar to that shown in Fig. 5a of Ref. [15]. In our case, the THz pulses were collimated and focused onto the sample by a pair of TPX lenses. Another pair of TPX lenses was relay imaging the sample position onto the detector photoconductive antenna. The peak of the amplitude spectrum of the broadband THz pulses was at about 0.65 THz. For the investigated strongly absorbing tissue samples, the useful spectral range was extending from about 0.2 to 2.0 THz. The THz pulses
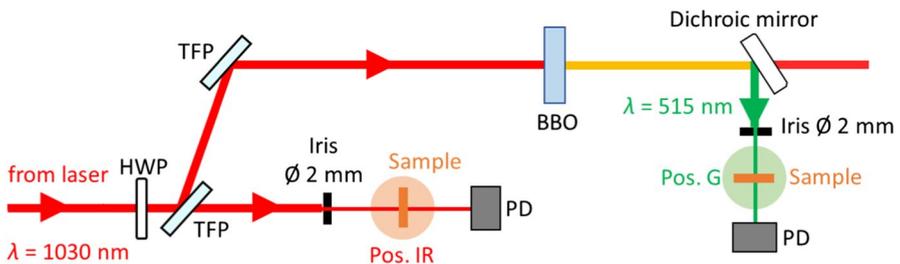

Fig. 1 Optical layout of the two-color optical irradiation setup. HWP half-wave retardation plate, TFP thin-film polarizer, PD photodiode

transmitted through the sample and the holder assembly (in reference measurements only through the holder assembly) were collimated and focused by another pair of TPX lenses onto a second, unbiased photoconductive antenna for waveform measurement. For this purpose, synchronized femtosecond laser pulses were overlapped with variable delay with the THz pulses on the photoconductive antenna.

2.2 Tissue Samples

Tissue samples were surgically isolated from earthworms *Eisenia andrei* (Annelida, Oligochaeta, Lumbricidae). Healthy, sexually matured (clitellated) specimens were used which were handsorted from the breeding stocks. For species identification, the mitochondrially encoded cytochrome c oxidase I (MT-CO1) gene sequestration was used. The selected specimens were kept on wetted paper wadding for three days to remove gut content. The samples were isolated from the middle part of the earthworm body (Fig. 2a).

For the optical transmission measurements, animals of different sizes were selected in order to provide dorsal body wall tissue samples of different thicknesses (d_{BW} = 0.17 mm, 0.23 mm, and 0.33 mm) but with the same structure (Fig. 2b). Pieces of the body wall of about 2.5 mm × 10 mm area were surgically isolated. The body wall contained the epithelial layer and the circular and longitudinal muscular layers. In addition, a sample containing the whole-body cross-section was also used with a thickness of 1.5 mm. After surgical isolation, the tissue samples were placed on 0.18-mm-thick glass plates (microscope cover plates, Fig. 2c and d) and covered by thin plastic tapes to prevent fast drying out. The plastic covering tape was
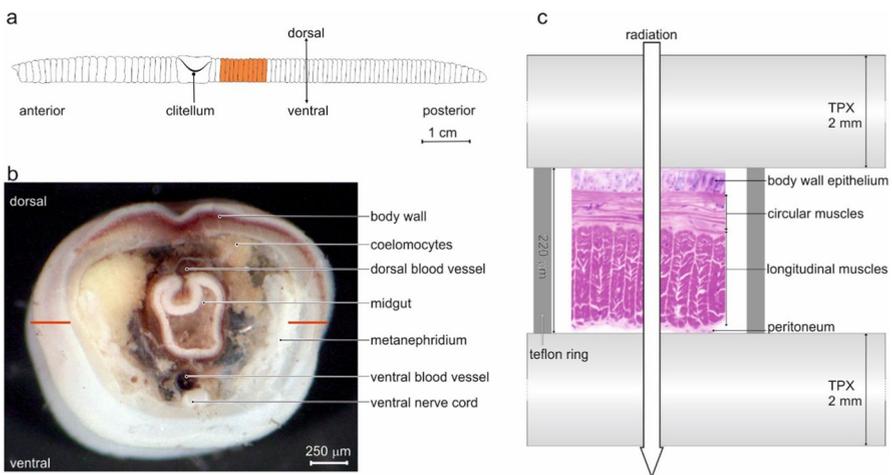
Fig. 2 **a** Schematic drawing of the earthworm *Eisenia andrei*. The coloring shows the part of the body from which the irradiated samples were prepared. **b** Photograph of the body cross-section of the earthworm. The red lines indicate the surgical cuts for tissue sample preparation. **c** Schematic drawing of the sample exposure arrangement with a body wall tissue of thickness d_{BW} (not to scale)

removed during the radiation transmission measurements. The thickness was measured on small pieces cut off from the sample by using an optical microscope with a scale. Optical transmission measurements were carried out one hour after sample preparation.

For the THz transmission measurements, dorsal body wall tissue samples of 0.22-mm and 0.33-mm thicknesses were used. Due to low transmission, results are shown here only for the thinner sample. After surgical isolation, the tissues samples were placed on 2-mm-thick polymethylpentene (PMP, often referred to as TPX) plates (Fig. 2d) and covered by another identical plate to prevent fast drying out. The sample thickness was precisely fixed by a Teflon spacer between the PMP plates.

3 Experimental Results

The power transmission $T(d)$ through a sample of thickness d was determined from measurements of the incoming and transmitted power according to the following approximate relation:

$$T(d) = \frac{P(d)}{T_g \cdot P_0}. \tag{1}$$

Here, P_0 is the incident power, $P(d)$ is the transmitted power through a sample of thickness d placed on the glass substrate with transmission T_g. The substrate transmission could not be measured directly when the sample was attached to it. Therefore, it was estimated from a reference measurement of the substrate in air, thus including reflection losses from two air-glass surfaces and the absorption losses in the bulk of the glass material. Consequently, $T(d)$ includes the absorption losses within the tissue and the (reflection and scattering) losses at the input air-tissue boundary surface (see also Eq. (2)).

Figure 3 shows, on a logarithmic scale, the measured power transmission for the green and IR laser pulses of 515-nm and 1030-nm central wavelengths, respectively, as functions of the sample tissue thickness. The measurements were carried out about 1 h after surgical isolation of the tissues from the earthworms. At the shorter wavelength of 515 nm, the attenuation is relatively strong and uniform. The transmitted power shows a simple exponential dependence on the tissue thickness to a reasonably good approximation (Fig. 3a; see also "Discussion" section). This indicates similar absorption properties for the body wall (0.17–0.33-mm thickness) and the inner part of the body (1.5 mm). About 66% of the radiation is transmitted through a 0.33-mm-thick body wall, and only about 22% of the incoming power is transmitted through the 1.5-mm-thick sample containing the whole-body cross-section.

The dependence on the sample thickness of the transmitted IR power through the body wall (up to 0.33-mm thickness) is similar to the case of the green light (Fig. 3b). About 74% of the incoming IR radiation is transmitted through 0.33 mm of body wall. However, the IR transmission through the body center is significantly larger than for green. About 50% of the IR radiation is transmitted through a 1.5-mm-thick sample with the full-body cross-section. Thus, there is a noticeable
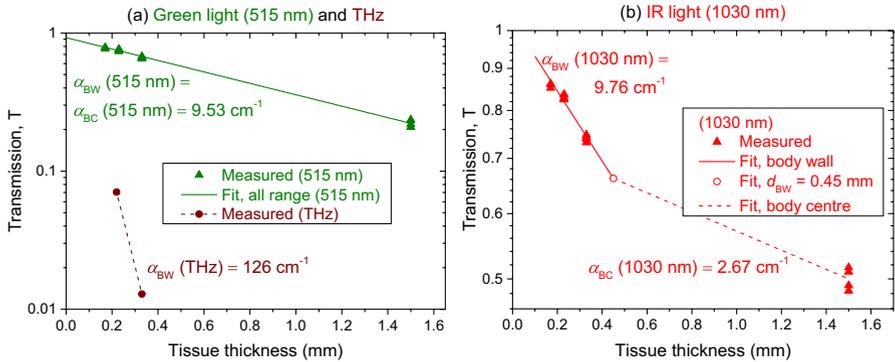
Fig. 3 **a** Measured power transmission for green light and THz radiation as function of the sample tissue thickness. **b** Measured power transmission for infrared light as function of the sample tissue thickness. The lines corresponding to green and IR indicate exponential fit curves. The dashed line in case of the THz data is a guide to the eye. The empty symbol in **b** indicates the body wall fit extrapolated to 0.45-mm thickness

difference between the transmission of the body wall and that of the body center, in contrast to green light.

Figure 4a shows the time dependence of the electric field strength of the transmitted THz pulses as function of time, measured by TDTS. The body wall tissue sample had a thickness of 0.22 mm (red curve). The reference pulse was passing through the empty sample holder assembly (black curve). The measurement was carried out about 1 h after surgical isolation of the samples. We note that over a time interval of 2 h, less than 3% relative change in the THz transmission was observed, thus covering the sample efficiently prevented it from drying out. The electric fields, shown in
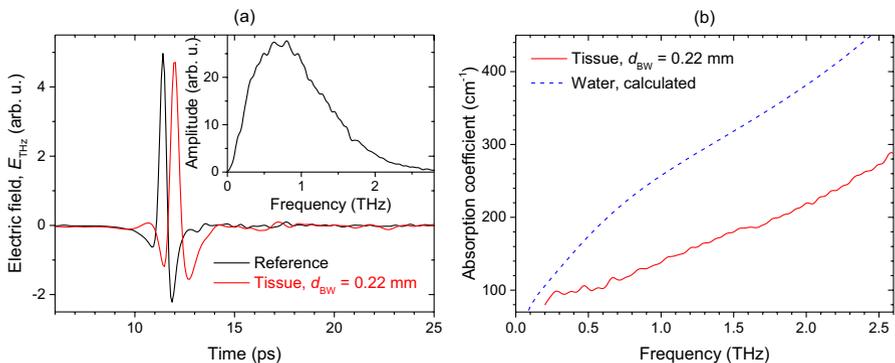
Fig. 4 **a** Electric field strength of the transmitted THz pulses as function of time, measured by TDTS. The body wall tissue sample had a thickness of 0.22 mm (red curve). The reference pulse was passing through the empty sample holder assembly (black curve). The inset shows the amplitude spectrum of the transmitted reference pulse. **b** Intensity absorption coefficient of the body wall as function of the THz frequency, calculated from the measured THz waveforms. The calculated absorption coefficient of water [16, 17] is shown for comparison

arbitrary units, are multiplied by different constant values for better comparability. The frequency-dependent intensity absorption coefficient of the body wall, calculated from the measured THz waveforms after Fourier transformation, is shown in Fig. 4b as function of the THz frequency.

It is possible to calculate the spectrally integrated power transmission for the THz pulses from the TDTS measurements. Figure 3a includes such THz power transmission values for two different body wall tissue thicknesses of 0.22 mm and 0.33 mm. The transmission was calculated by taking the ratio of the relative power of THz pulses with and without sample. Relative power values were obtained by integrating the power spectra from the TDTS measurements from 0.15 to 2.5 THz. The THz power transmission, calculated in this way, gives a body-wall absorption coefficient of 126 cm^{-1} (Fig. 3a). This coincides well with the average absorption coefficient in the range of about 0.5 to 1 THz (Fig. 4b). The reason of this coincidence is the spectral amplitude maximum in this range (see inset in Fig. 4a).

4 Discussion

4.1 Tissue Absorption Coefficients

The purpose of the transmission measurements was to obtain values for α_{BW} and α_{BC}, the (average) absorption coefficients of the earthworm body wall and body center, respectively. The measured dependence of the power transmission T (defined in Eq. (1)) on the sample thickness and structure was approximated by the fit function

$$T\left(d = d_{BW} + d_{BC}\right) = \tau \cdot e^{-\alpha_{BW} \cdot d_{BW}} \cdot e^{-\alpha_{BC} \cdot d_{BC}}. \tag{2}$$

Here, d, d_{BW}, and d_{BC} are the thicknesses of the full sample, the body wall, and the body center, respectively. The thinner samples (up to 0.33-mm thickness) were composed of body wall tissue only, therefore, $d = d_{BW}$ holds in these cases. For the sample containing the full-body cross-section, the full thickness was $d = d_{BW} + d_{BC}$ = 1.5 mm, with $d_{BW} = 0.45$ mm and $d_{BC} = 1.05$ mm. Note that in this case, d_{BW} refers to the total thickness of the dorsal and the ventral body walls. In Eq. (2), τ denotes the losses at the input air-tissue boundary surface, as already mention in connection to Eq. (1).

The IR absorption coefficients were obtained by the following fitting procedure. First, the model function given by Eq. (2) was used with $d_{BC} = 0$ to determine α_{BW} from the measurements with the thinner samples composed of body wall only. Then, a second fit was carried out with $d_{BW} = 0.45$ mm and $d_{BC} = 1.05$ mm, with α_{BC} as the only free parameter. In this case, only the measured data for the sample with full body cross-section were considered.

The results of the curve fitting, together with the obtained absorption coefficient values, are shown in Fig. 3a for green light and in Fig. 3b for IR light. Numerical values of the tissue absorption coefficients for all three radiation types are summarized in Table 1. As mentioned earlier, all absorption coefficients correspond to

Table 1 Measured absorption coefficients of the *Eisenia andrei* body wall tissue samples for green and IR light and for a few selected THz frequencies. For THz radiation, average values for two frequency intervals are also given, which are considered in the discussion

Wavelength, λ (nm) or frequency, ν (THz)	Absorption coefficient, α_{BW} (cm^{-1})
515 nm	10.6
1030 nm	9.8
0.2 THz	80
0.3 THz	97
0.5 THz	102
1.0 THz	138
1.5 THz	180
2.0 THz	220
2.5 THz	273
0.2–0.5 THz	97 (average, used in heat calculation)
0.15–2.5 THz	126 (average, Fig. 3a)

measurements carried out 1 h after surgical removal of the tissue samples from the animals.

For green light of 515-nm wavelength, the fitting procedure as described above delivers nearly equal absorption coefficients for the body wall and the body center ($\alpha_{BW} = 10.6$ cm^{-1} and $\alpha_{BC} = 9.2$ cm^{-1}, respectively; not shown in Fig. 3a). Hence, a good agreement for all sample thicknesses can be obtained by using a simplified fit function with identical values for both absorption coefficients (Fig. 3a). This delivers the value $\alpha_{BW} = \alpha_{BC} = 9.5$ cm^{-1}.

For IR light of 1030-nm wavelength, it is necessary to use different absorption coefficients for the body wall and the body center (Fig. 3b). The fitting procedure delivers $\alpha_{BW} = 9.8$ cm^{-1} (Table 1) and $\alpha_{BC} = 2.7$ cm^{-1}, respectively. The body wall absorption coefficient is very similar to that for the green light, but for the body center, it is about 3.5 times smaller. We note that a moderate increase of the IR body wall absorption coefficient with increasing thickness can be observed (Fig. 3b).

In the THz range, the frequency-dependent absorption coefficient of the body wall was determined from the TDTS measurements. First, the amplitude spectra $E_s(\omega)$ and $E_r(\omega)$ were calculated by Fourier transformation from the measured temporal waveforms with the tissue sample and the reference without the sample, respectively. The absorption coefficient was calculated from the following formula [15]:

$$\alpha_{BW}(\omega) = -\frac{2}{d_{BW}} ln \left[\frac{\left| E_s(\omega) \right|}{\left| E_r(\omega) \right|} \right]. \tag{3}$$

Concerning the interfaces and surfaces, the difference between the reference and the sample measurements only is that the two inner interfaces are TPX-air (and air-TPX) for the reference measurement, whereas they are TPX-tissue (and tissue-TPX) for sample the measurement. Near 0.2 THz, above which our TDTS measurements are considered to be reliable, the tissue refractive index is estimated to be smaller than 2.5 and it is rapidly decreasing to values near 2 with increasing frequency (see

Ref. [12] for comparison with other tissue types). Since the ratios of the refractive indices of the materials on the two sides of the interfaces are about the reciprocals of each other, the caused Fresnel losses are about the same. More precisely, with the refractive indices $n_{TPX} = 1.46$ for TPX, $n_{air} = 1$ for air, and $n_{BW} = 2$ (2.5) for the body wall tissue, we obtain a relative error in the calculated tissue absorption coefficient of less than 1% (3%) for the investigated sample thicknesses. This is smaller than the estimated uncertainty of 10 to 15% originating from sample-by-sample variation and the limited thickness measurement accuracy.

The obtained intensity absorption coefficient for the body wall is plotted in Fig. 4b as function of the THz frequency. It steadily increases from about 80 cm^{-1} at 0.2 THz to about 220 cm^{-1} at 2.0 THz. For comparison, the absorption coefficient of pure water increases from about 106 cm^{-1} at 0.2 THz to about 382 cm^{-1} at 2.0 THz [16, 17]. The absorption coefficient of pure water, calculated from a room temperature dispersion formula [16, 17], also can be seen in Fig. 4b. Thus, the absorption coefficient of the tissue samples measured here is about 60 to 75% of that of pure water. The water content of *Eisenia andrei* specimens was measured to be 81.5% (82.7%) in the anterior (postclitellar) part of the body. The measured tissue and the calculated water absorption coefficients are given for a few selected THz frequencies in Table 1 (cf. Fig. 3a as well).

4.2 Estimation of the Heating Effect

The simplest direct effect of radiation on a tissue can be heating due to the absorbed power. A steady-state heat equation was used to model the heating effect of radiation on the tissue and to compare it to pure water. The beam was assumed to propagate into the z direction. For the sake of simplicity, temperature variation only in z direction was considered. Such an approximation is suitable for the body-wall tissue, where the thickness of the tissue (0.22 mm in this case) is significantly smaller than its lateral size (≥ 2.5 mm) and the typical size of a focused THz beam (≥ 2 mm for frequencies of 0.2–0.5 THz). Furthermore, a homogeneous medium was assumed with the absorption coefficient $\alpha_{BW} = 97$ cm^{-1}. This corresponds to the average measured absorption coefficient of the body wall tissue in the 0.2 to 0.5 THz range. This choice is justified by the spectral band of the most intense part of the THz pulses used in our previous study [6]. The following one-dimensional heat equation was solved (see, e.g., Refs. [18–20]):

$$\Delta T(z) = \frac{\partial^2}{\partial z^2} T(z) = -\frac{1}{k} q(z). \tag{4}$$

Here, $T(z)$ is the steady-state temperature at tissue depth z. The thermal conductivity k was assumed to be constant, i.e., independent of temperature and position. Temperature independence is justified by the small increases in temperature, as discussed below.

For the thermal conductivity of the body-wall tissue sample, an estimated value of $k = 0.50$ W m^{-1} K^{-1} was used here. For comparison, the room-temperature (293 K) thermal conductivity of water is 0.60 W m^{-1} K^{-1} [21]. We note that

thermal conductivity values reported in the literature for biological tissues vary in a broad range. The values depend on species, tissue type, in vivo or in vitro conditions, temperature [19], hydration level, and other circumstances. For example, for in vivo conditions, blood circulation can have a substantial effect [22]. Typical reported in vivo values for animal skin or muscle tissues are in the range 0.5–0.6 W m^{-1} K^{-1} [19, 20, 22, 23].

In case of heating caused by radiation absorption, the dissipated power density in unit W m^{-3} is given by $q(z) = \alpha_{BW} I_0 \exp(-\alpha_{BW} z)$, where I_0 (of unit W m^{-2}) is the average intensity at $z = 0$. The boundary conditions were defined as follows:

$$\frac{\partial}{\partial z}\bigg|_{z=0} T(z) = 0, \tag{5}$$

$$T(d_{BW}) = T_a. \tag{6}$$

It was assumed that there is no heat loss to air or other surrounding medium at the entrance side of the sample ($z = 0$), which is expressed by Eq. (5). At the back side of the sample, the glass substrate was considered to act as a heat sink at the constant ambient temperature T_a, as described by Eq. (6). Because this assumption overestimates the effect of the glass substrate and other effects, such as heat loss by air convection, are neglected, the temperature values given below can be regarded as an estimation of the order of magnitude for the heating effect of THz radiation. The solution of the heat Eq. (4), obeying such boundary conditions, can be given as:

$$T(z) = T_a + \frac{I_0}{k}(d_{BW} - z) + \frac{I_0}{\alpha_{BW} k}\left(e^{-\alpha_{BW} d_{BW}} - e^{-\alpha_{BW} z}\right). \tag{7}$$

The calculated results for the THz intensity and the temperature increase are shown in Fig. 5 for the case of THz radiation propagating through 0.22-mm thickness of body wall. The incident average intensity inside the tissue was assumed to be about 160 mW cm^{-2}. This corresponds to the situation used in our previous work [6] with 5-μJ pulse energy, 1-kHz repetition rate, and 1-mm focused THz beam radius, giving 5-mW average input power. About 12% of THz radiation is transmitted through the sample (Fig. 5a). The largest increase in sample temperature of 0.41 K is obtained at the input surface $z = 0$ (Fig. 5b). Such a small temperature increase suggests that heating may have negligible effect on biological functions. Comparison with pure water (with an average absorption coefficient of 141 cm^{-1} in the 0.2 to 0.5 THz range) shows very similar temperature increase, due to the similar absorption coefficient of water. For comparison, Fig. 5 also shows the intensity and temperature increase as functions of the penetration depth for the green and IR optical radiations. These data were calculated with the measured body wall absorption coefficients as given in the first two rows of Table 1, whereby the same 160-mW cm^{-2} average input intensity was assumed as in case of the THz radiation. For optical radiation, the penetration depth is much larger (about 1 mm) and the temperature increase is even smaller (less than 0.1 K).
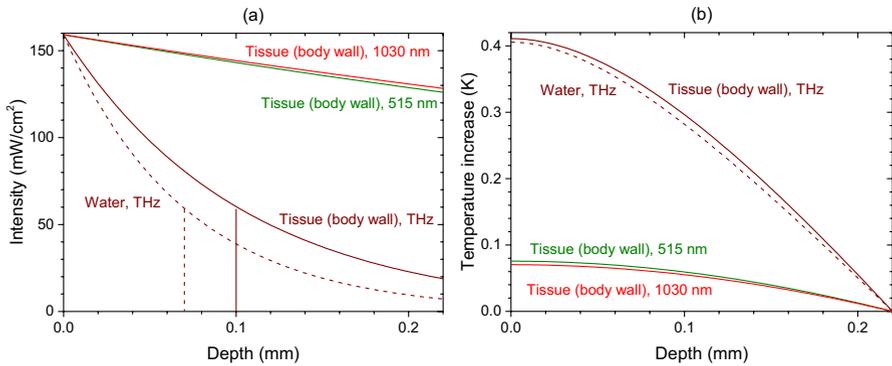
Fig. 5 Calculated intensity (**a**) and temperature increase (**b**) in body wall tissue caused by irradiation with THz, green, and IR pulses. The dashed lines show the calculation for pure water and THz radiation. Both for the tissue and water, THz average absorption coefficients ($\overline{\alpha}$) for the 0.2 to 0.5 THz range were used. The vertical lines show the THz penetration depths ($1/\overline{\alpha}$) in tissue (solid line) and water (dashed line)

Based on the small (about 0.4 K) estimated temperature elevation, the observed very pronounced stimulation of segment regeneration by THz irradiation [6] could be dominated by effects other than heating. However, we note that the temperature increase is proportional to the incident power or intensity according to Eqs. (4) and (7). Because of this, current cutting-edge high-intensity THz sources with mJ-level pulse energies (see e.g. Ref. [24]) can have very significant direct heating effects of tens-of-K, especially for high repetition rates and/or long exposure times.

5 Conclusion

Transmission of green (515 nm), near-infrared (1030 nm), and THz pulses through biological tissue was studied. As model, tissue samples taken from *Eisenia andrei* earthworms of different sizes were used, containing the epithelial layer and the circular and longitudinal muscles. Also samples of larger thickness, containing the complete cross-section of the animal, were investigated for comparison. Whereas the transmitted power for the green optical pulses reasonably followed the Beer-Lambert law of exponential attenuation for all thicknesses and tissue structures, near-infrared pulses were significantly deviating from this, which hints to the dependence on tissue structure. The tissue absorption coefficient was measured by time-domain THz spectroscopy in the frequency range from 0.2 to 2.5 THz. The absorption varies from 80 cm^{-1} at 0.2 THz to 273 cm^{-1} at 2.5 THz.

Simple model calculations indicate that THz pulses of 5-μJ energy and 1-kHz repetition rate (5-mW average power), as used in Ref. [6], cause a small temperature increase of about 0.4 K, suggesting that the reason of the dramatic biological effect reported in Ref. [6] cannot be a simple heating of the earthworms. This can be drastically different for mJ-level THz pulse energies, which have become available recently.

The knowledge of tissue absorption properties is an important prerequisite to estimate the biological effectiveness of radiation. It can also set the framework to investigate in detail the mechanisms of various biological effects. Intense pulsed THz radiation can have a profound biological impact. Despite small penetration depths of about 0.1 mm for the 0.2 to 2.5 THz range considered in the present work, global (nonthermal) biological effects can occur. For example, in our previous study, a very pronounced influence of THz irradiation on the tail regeneration of *Eisenia andrei* earthworms was found [6]. In this context, it is also of interest to extend the absorption measurements to still lower frequencies, where the penetration depth can be larger. It can be anticipated that global, organism-level effects can occur in other types of living creatures, even in case of larger-sized organisms.

Data Availability Contact the corresponding author.

Code Availability Not applicable.

Declarations

Conflicts of Interest The authors declare no conflicts of interest.

References

1. M.R. Hamblin, Y.-Y. Huang, V. Heiskanen, Non-mammalian hosts and photobiomodulation: Do all life-forms respond to light?, Photochemistry and Photobiology 95 (2019) 126-139.
2. K.M. AlGhamdi, A. Kumar, N.A. Moussa, Low-level laser therapy: a useful technique for enhancing the proliferation of various cultured cells, Lasers in Medical Science 27 (2012) 237-249.
3. O.P. Cherkasova, D.S. Serdyukov, A.S. Ratushnyak, E.F. Nemova, E.N. Kozlov, Y.V. Shidlovskii, K.I. Zaytsev, V.V. Tuchin, Effects of terahertz radiation on living cells: A review, Optics and Spectroscopy 128 (2020) 855-866.
4. L.V. Titova, A.K. Ayesheshim, A. Golubov, R. Rodriguez-Juarez, R. Woycicki, F.A. Hegmann, O. Kovalchuk, Intense THz pulses down-regulate genes associated with skin cancer and psoriasis: A new therapeutic avenue?, Scientific Reports 3 (2013) 2363.
5. M.M. Nazarov, A.P. Shkurinov, E.A. Kuleshov, V.V. Tuchin, Terahertz time-domain spectroscopy of biological tissues, Quantum Electronics 38 (2008) 647-654.

6.   M.H. Abufadda, A. Erdélyi, E. Pollák, P.S. Nugraha, J. Hebling, J.A. Fülöp, L. Molnár, Terahertz pulses induce segment renewal via cell proliferation and differentiation overriding the endogenous regeneration program of the earthworm Eisenia andrei, Biomedical Optics Express 12 (2021) 1947-1961.

7.   S.W. Smye, J.M. Chamberlain, A.J. Fitzgerald, E. Berry, The interaction between terahertz radiation and biological tissue, Physics in Medicine and Biology 46 (2001) R101-R112.

8.   S. Romanenko, R. Begley, A.R. Harvey, L. Hool, V.P. Wallace, The interaction between electromagnetic fields at megahertz, gigahertz and terahertz frequencies with cells, tissues and organisms: Risks and potential, Journal of The Royal Society Interface 14 (2017) 20170585.

9.   E. Pickwell, V.P. Wallace, Biomedical applications of terahertz technology, Journal of Physics D: Applied Physics 39 (2006) R301-R310.

10.   A.J. Fitzgerald, E. Berry, N.N. Zinov'ev, S. Homer-Vanniasinkam, R.E. Miles, J.M. Chamberlain, M.A. Smith, Catalogue of human tissue optical properties at terahertz frequencies, Journal of Biological Physics 29 (2003) 123-128.

11.   F.H. Mustafa, M.S. Jaafar, Comparison of wavelength-dependent penetration depths of lasers in different types of skin in photodynamic therapy, Indian Journal of Physics 87 (2013) 203-209.

12.   X.G. Peralta, D. Lipscomb, G.J. Wilmink, I. Echchgadda, Terahertz spectroscopy of human skin tissue models with different melanin content, Biomedical Optics Express 10 (2019) 2942-2955.

13.   A. Amaroli, S. Ferrando, M. Pozzolini, L. Gallus, S. Parker, S. Benedicenti, The earthworm Dendrobaena veneta (Annelida): A new experimental-organism for photobiomodulation and wound healing, European Journal of Histochemistry 62 (2018) 51-61.

14.   A. Amaroli, S. Ferrando, R. Hanna, L. Gallus, A. Benedicenti, S. Scarfì, M. Pozzolini, S. Benedicenti, The photobiomodulation effect of higher-fluence 808-nm laser therapy with a flat-top handpiece on the wound healing of the earthworm Dendrobaena veneta: A brief report, Lasers in Medical Science 33 (2018) 221-225.

15.   P.U. Jepsen, D.G. Cooke, M. Koch, Terahertz spectroscopy and imaging – Modern techniques and applications, Laser & Photonics Reviews 5 (2011) 124-166.

16.   M. Nagai, H. Yada, T. Arikawa, K. Tanaka, Terahertz time-domain attenuated total reflection spectroscopy in water and biological solution, International Journal of Infrared and Millimeter Waves 27 (2006) 505-515.

17.   Y.-S. Lee, Principles of terahertz science and technology (Springer, New York, NY, 2009).

18.   T.T.L. Kristensen, W. Withayachumnankul, P. Uhd Jepsen, D. Abbott, Modeling terahertz heating effects on water, Optics Express 18 (2010) 4727–4739.

19.   C. Rossmanna, D. Haemmerich, Review of temperature dependence of thermal properties, dielectric properties, and perfusion of biological tissues at hyperthermic and ablation temperatures, Critical Reviews in Biomedical Engineering 42 (2014) 467-492.

20.   K. Giering, O. Minet, I. Lamprecht, G. Müller, Review of thermal properties of biological tissues, Proceedings of SPIE 25 (1995) 45-65.

21.   M.L.V. Ramires, C.A. Nieto de Castro, Y. Nagasaka, A. Nagashima, M.J. Assael, W.A. Wakeham, Standard reference data for the thermal conductivity of water, Journal of Physical and Chemical Reference Data 24 (1995) 1377-1381.

22.   L. Li, M. Liang, B. Yu, S. Yang, Analysis of thermal conductivity in living biological tissue with vascular network and convection, International Journal of Thermal Sciences 86 (2014) 219-226.

23.   T. Kujawska, W. Secomski, E. Kruglenko, K. Krawczyk, A. Nowicki, Determination of tissue thermal conductivity by measuring and modeling temperature rise induced in tissue by pulsed focused ultrasound, PLOS ONE 9 (2014) e94929.

24.   C. Vicario, A.V. Ovchinnikov, S.I. Ashitkov, M.B. Agranat, V.E. Fortov, C.P. Hauri, Generation of 0.9-mJ THz pulses in DSTMS pumped by a Cr:Mg$_2$SiO$_4$ laser, Optics Letters 39 (2014) 6632–6635.